A penalized weighted least-squares image reconstruction based on scatter correction methods for X-ray CT

Long Chen, Thomas Rodet, Nicolas Gac

A Penalized Weighted Least-Squares Image Reconstruction based on Scatter Correction Methods for X-ray CT

Long Chen, Thomas Rodet, and Nicolas Gac

Abstract—For metal artifact reduction (MAR) in X-ray cone-beam computed tomography (CBCT), we propose a penalized weighted least-squares (PWLS) image reconstruction method [1] based on scatter correction (SC) method. Our main contribution is to incorporate the inaccuracy of the scatter correction data in PWLS method, and to accelerate the PWLS image reconstruction with a preconditionned conjugate gradient (PCG) method [2]. The reconstruction results of both the simulation and experimental data show that our proposed method effectively reduces the metal artifacts (MA). Compared to the state of art, normalized metal artifact reduction (NMAR) method [3], our method prevents the introduction of some new artifacts due to an inapporiate interpolation possible used in NMAR.

I. INTRODUCTION

In X-ray CBCT, beam hardening, scatter, noise and exponential edge-gradient effect are major causes of the metal artifacts [4]. The scatter correction is crucial to MAR and restoration of contrast loss in the reconstructed images, and also very important in the case of 3D tomography with flat panel detector. In this abstract, we only take account of the scatter influence for MAR. For the reduction of the beam-hardening artifacts, a new multi-energy map approach was proposed in [5].

One of the main groups of SC methods is the measurement-based methods (beam stop (BS) [6] and collimator shadow [7]). These methods assume a smooth distibution for scatter, and estimate the scatter from the detectors where the scatter only contributes to the measurements. They may degrade the reconstructed images, as the result of ignoring the high-frequency scatter noise [6].

In X-ray CBCT, dense metal, like dental metallic fillings or implants, can stop a beam of X-ray in some projections, similar to BS array. So we proposed a mesurement-based method for SC. Our MAR stategy contains two steps, SC correction and PWLS image reconstruction. The inaccuracy of SC is taken account of in PWLS image reconstruction, detailed in the next section. Furthermore, the PWLS image reconstruction is accelerated by PCG.

The organization of the rest paper is as follow: the next section describes our method, our reconstruction results of

Long Chen is with the Laboratory of Signals and Systems, UMR8506, Université Paris-Sud-CNRS-Supélec, Gif-sur-Yvette cedex, F-91192, France

Thomas Rodet is with the Departement of Electronics, Electrotechnics and Automatics, Ecole Normalienne Supérieur de Cachan, Cachan cedex, F-94235, France

Nicolas Gac is with the Laboratory of Signals and Systems, UMR8506, Université Paris-Sud-CNRS-Supélec, Gif-sur-Yvette cedex, F-91192, France
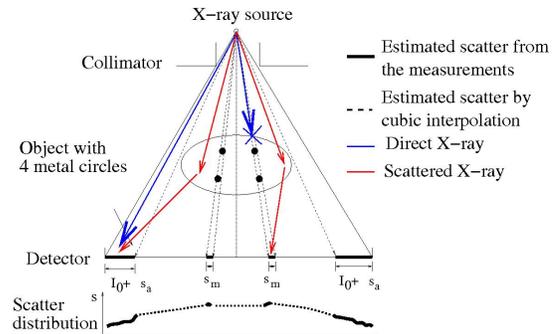
Fig. 1: Illustration of the proposed SC method in CBCT, s_A and s_M are the respective scatter distribution of air and metal projection.

simulation and real data are given in third section, and the final section is conclusion.

II. METHOD

In X-ray CBCT, according to Beer-Lambert's law, a simple mathematical model is used to describe the physical acquisition processus with scatter radiation below,

$$\mathbf{I} = I_0 * (e^{-\mathbf{Hf}} + \mathbf{s}(\mathbf{f})) + \mathbf{I}_\epsilon \qquad (1)$$

where $\mathbf{I}$ is the measured intensity of X-ray by detector, I_0 is the incident intensity of X-ray, $\mathbf{f}$ and $\mathbf{H}$ are assigned to the unknowned X-ray attenuation vector and the forward system matrix, and we also call $\mathbf{H}$ projector. $\mathbf{s}$ and $\mathbf{I}_\epsilon$ are the scatter factor depending on $\mathbf{f}$ and the noise vector, respectively.

Our proposed MAR method based on SC consists of two steps, scatter correction and PWLS image reconstruction. Our SC method is described in Fig.1. The primary signal measurements [6], $\mathbf{p} = I_0 * e^{-\mathbf{Hf}}$, are estimated by substraction of the obtained scatter values from the original measurements. By pre-processing the SC measurements with negative logarithm, we obtain a linear relation between the unknown vector $\mathbf{f}$ and the corrected data $\mathbf{g}$ as follow:

$$\mathbf{g} = \mathbf{Hf} + \epsilon \qquad (2)$$

where ϵ stands for noise and the modelling error. We assume ϵ to be gaussian. The objective function of PWLS is defined as follow:

$$J(\mathbf{f}) = (\mathbf{g} - \mathbf{Hf})^T \mathbf{W}(\mathbf{g} - \mathbf{Hf}) + \beta\Phi(\mathbf{f}) \qquad (3)$$
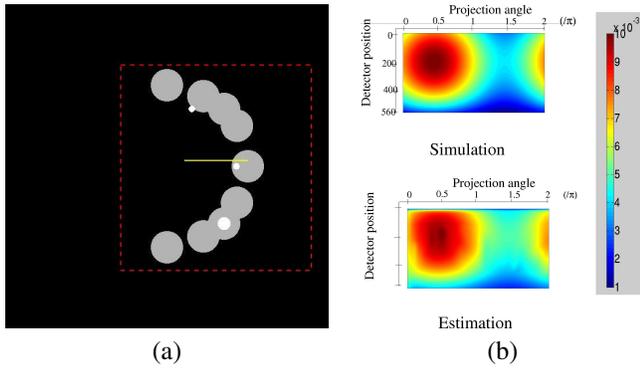
Fig. 2: The simulated phantom (a) and scatter distribution (b).

where the weighted matrix, $\mathbf{W}$, is determined by the measurement variance [1] and the inaccuracy of the SC. Smaller weights are distributed to the SC data of metal projection and its neigbouring projection, since the metal measurements have greater variance and the SC data of the neighbouring pixel of metal is less confident. The smoothing parameter, β, is chosen empirically, and the Huber function is used as the penalty function, $\Phi(\mathbf{f})$, which is defined as follow:

$$\Phi_H(t) = \begin{cases} t^2, & si \ |t| \le \delta_H \\ 2|t|\delta_H - \delta_H^2, & si \ |t| > \delta_H \end{cases} \quad (4)$$

where δ_H is the threshold of Huber function.

Using the weighted matrix $\mathbf{W}$, the PWLS image reconstruction converges more slowly than the penalized least-squares (PLS) image reconstruction. In order to accelerate the PWLS image reconstruction, we employ a preconditioned conjugate method [2]. A preconditioning matrix is used to compensate the influence of the weight matrix in the convergence rate of image reconstruction. We change variable using the preconditioning matrix $\mathbf{M}$ by $\mathbf{f} = \mathbf{Mf}'$. The objective function is modified as below:

$$J(\mathbf{f}') = (\mathbf{g} - \mathbf{HMf}')^t \mathbf{W}(\mathbf{g} - \mathbf{HMf}') + \lambda\Phi(\mathbf{f}') \quad (5)$$

To find a solution of $\mathbf{f}$, we only need to know the $\mathbf{MM}^t$ instead of $\mathbf{M}$ using PCG ([2]). $\mathbf{MM}^t$ is given below:

$$\mathbf{MM}^t = \mathbf{H}^t \mathbf{1}(\mathbf{H}^t \mathbf{W} \mathbf{1})^{-1} \quad (6)$$

where $\mathbf{H}^t$ is our backprojector, and $\mathbf{1}$ is a vector filled with ones.

III. RESULTS

Our proposed method has been evaluated by both the simulation and experimental data.

In simulation study, we used a jaw-like simulated phantom (Fig.2.a), containing 2 materials, bone and copper. The scatter distribution is dependent on the scanned object, so we simulated it by varying the scatter distribution on function of the projection view position, in Fig.2.b. We generated the simulation data with use of our projector and added the scattered contribution. Our SC method gives a good estimation in Fig. 2.b. For comparison, a PLS method is employed in image reconstruction. Compared to PLS reconstruction
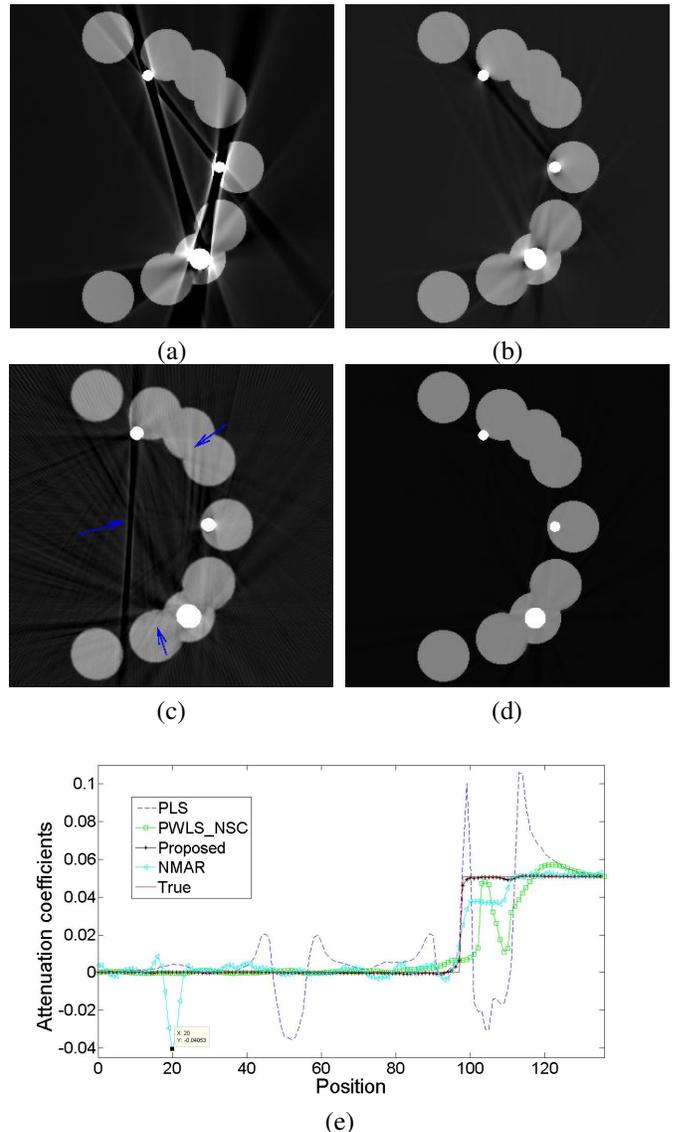

Fig. 3: The reconstructed images by different methods in display window [-0.01 0.1]: (a) PLS without SC (PLS_NSC), (b) PWLS without SC (PWLS_NSC), (c) NMAR, (d) our proposed method, and (e) Profiles of the yellow lines in Fig.2. In (c), the blue arrows indicate the new artifacts introduced by NMAR.

without SC (PLS_NSC in Fig.3.a), the PWLS method Without SC reduces the MAs connecting each two copper circles, but fails to the MAs around the metal circles (PWLS_NSC in Fig.3.b). The NMAR is able to remove the black and white streaks connecting each two copper circles, however, it introduces some new artifacts (Fig.3.c). On the benifits of the scatter correction, our proposed method suppresses both of them and gives the best reconstruction (Fig.3.d). The profile results in Fig.(3.e) prove the superiority of our proposed method as well. The PWLS image reconstruction is well accelerated by PCG, we just need 300 iterations, instead of 600 for standard PWLS method, in Fig.4, to obtain an MA-free image (Fig.3.c). Each iteration of the PCG-PWLS image
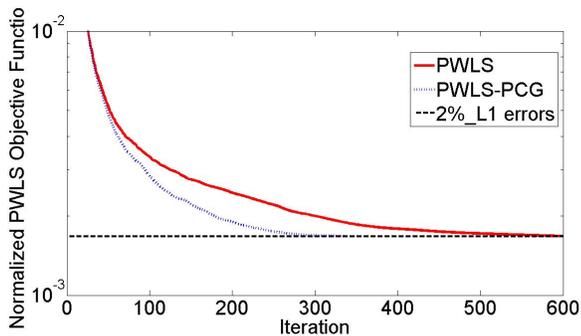
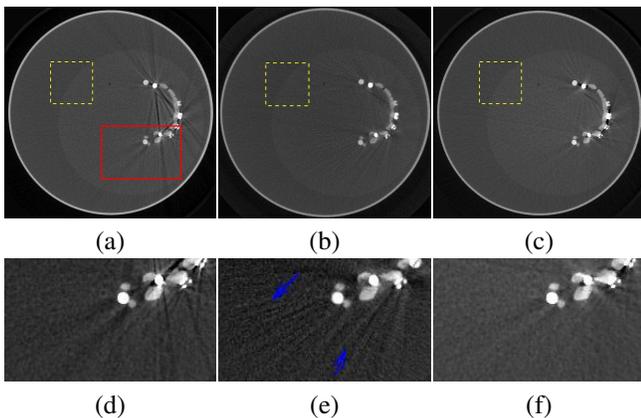Fig. 4: Convergence of iterative reconstructions using standard PWLS method and PWLS accelerated by PCG.

Fig. 5: The reconstructed images (576^2) of the real dataset (457 projections with 560 detector array) with display window [-0.01 0.08]: (a) PLS without SC, (b) NMAR, (c) our proposed method. Their zooms in red rectangle (Fig. 5.a) are given in (d) PLS without SC, (e) NMAR et (f) our proposed method. In (e), the blue arrows indicate the new artifacts introduced by NMAR.

reconstruction contains only two multiplications of matrix more than one of the standard PWLS, so the computation time of one iteration in the PCG-PWLS and the standard PWLS is almost the same. An MA-free image is obtained when the $L1$ error goes below certain criteria, for exemple, 2%. The $L1$ error is defined as follow:

$$e_{L1} = \|\hat{f} - f^*\|_1 / \|f^*\|_1 \qquad (7)$$

where $\hat{f}$ stands for an reconstructed image, f^* is the true image, and $\| \bullet \|_1$ is the $L1$ norm.

We also applied our proposed method to a real dataset of the experimental jaw-like phantom with metal caps and implants acquired with a commercial dental X-ray scanner. The same conclusion above is found in the real data results. Moreover, our method definitely improves the contrast in the yellow dashed rectangle zone (Fig.5.a), which contains two materials (water and equivalent plastique tissu) with close attenuation coefficients. The contrast is defined by the difference of the mean of the attenuation coefficients of two neighbouring materials [6]. Numerically, the contrast of the yellow dashed rectangle zone (Fig.5.a) is $2.0 * 10^{-3} \ mm^{-1}$, as well as in the

NMAR recontructed image (Fig.5.b), that of our reconstructed image (Fig.5.c) is $4.0 * 10^{-3} \ mm^{-1}$. In fact, the difference of the measured attenuation coefficients of water and equivalent plastique tissu is $4.4 \sim 4.9 * 10^{-3} \ mm^{-1}$.

IV. Conclusion

We have proposed a PWLS method based on scatter correction for the purpose of MAR. The reconstruction results of both the simulation and experimental data have shown the efficacy of our proposed method on MAR. Meanwhile, our method doesn't introduce some new artifacts caused by a local unfit interpolation in NMAR. Thanks to the acceleration by PCG, our PWLS image reconstruction algorithm can be employed with a more reasonable processing time.

In our reconstructed image of real data, there are still a few small black spots around the metal . To our knowledge, the rest black spots may be contributed by others main causes of MA, like beam-hardening, Therefore, our future work is to take account of them for the removel of the rest metal artifacts.

References

[1] Jeffrey A. Fessler, "Penalized weighted least-squares image reconstruction for positron emission tomography," *IEEE Trans. Med. Imag.*, vol. 13, no. 2, pp. 290–300, 1994.

[2] Jorge Nocedal and Stephen J. Wright, *Numerical Optimization*, Springer Ser. Oper. Res. Financ. Eng. Springer, New York, 2006.

[3] E. Meyer, R. Raupach, M. Lell., B. Schmidt., and M. Kachelrie, "Normalized metal artifact reduction (nmar) in computed tomography," *Med. Phys.*, vol. 37, no. 9, pp. 5482, 2010.

[4] B. De Man, J. Nuyts, P. Dupont, G. Marchal, and P. Suetens, "Metal streak artifacts in x-ray computed tomography: A simulation study," *IEEE Trans. Nucl. Sci.*, vol. 46, no. 3, pp. 691–696, 1999.

[5] Y. Zheng, C. Cai, and T. Rodet, "Joint reduce of metal and beam hardening artifacts using multi-energy map approach in x-ray computed tomography," in *Acoustics, Speech and Signal Processing (ICASSP), 2011 IEEE International Conference on*, 2011, pp. 737 – 740.

[6] L. Zhu, J. Wang, and L. Xing, "Noise suppression in scatter correction for cone-beam ct," *Med. Phys.*, vol. 36, no. 3, pp. 741–752, 2009.

[7] J. H. Siewerdsen, MJ. Daly, B. Bakhtiar, DJ. Moseley, S. Richard, H. Keller, and DA. Jaffray, "A simple, direct method for x-ray scatter estimation and correction in digital radiography and cone-beam ct," *Med. Phys.*, vol. 33, no. 1, pp. 187–197, 2006.